PHYSICAL REVIEW D **95,** 115034 (2017)

Probing a new strongly interacting sector via composite diboson resonances

P. Ko[*]
School of Physics, KIAS, Seoul 130-722, Korea

Chaehyun Yu[†]
Institute of Physics, Academia Sinica, Nangang, Taipei 11529, Taiwan, and Department of Physics, Korea University, Seoul 02841, Korea

Tzu-Chiang Yuan[‡]
Institute of Physics, Academia Sinica, Nangang, Taipei 11529, Taiwan

(Received 11 April 2016; revised manuscript received 23 January 2017; published 28 June 2017)

Diphoton resonance was a crucial discovery mode for the 125 GeV Standard Model Higgs boson at the Large Hadron Collider (LHC). This mode or the more general diboson modes may also play an important role in probing for new physics beyond the Standard Model. In this paper, we consider the possibility that a diphoton resonance is due to a composite scalar or pseudoscalar boson, whose constituents are either new hyperquarks Q or scalar hyperquarks $\tilde{Q}$ confined by a new hypercolor force at a confinement scale Λ_h. Assuming the mass m_Q (or $m_{\tilde{Q}}$) $\gg \Lambda_h$, a diphoton resonance could be interpreted as either a $Q\bar{Q}(^1S_0)$ state η_Q with $J^{PC}=0^{-+}$ or a $\tilde{Q}\tilde{Q}^\dagger(^1S_0)$ state $\eta_{\tilde{Q}}$ with $J^{PC}=0^{++}$. For the $Q\bar{Q}$ scenario, there will be a spin-triplet partner ψ_Q which is slightly heavier than η_Q due to the hyperfine interactions mediated by hypercolor gluon exchange; while for the $\tilde{Q}\tilde{Q}^\dagger$ scenario, the spin-triplet partner $\chi_{\tilde{Q}}$ arises from higher radial excitation with nonzero orbital angular momentum. We consider productions and decays of η_Q, $\eta_{\tilde{Q}}$, ψ_Q, and $\chi_{\tilde{Q}}$ at the LHC using the nonrelativistic QCD factorization approach. We discuss how to test these scenarios by using the Drell-Yan process and the forward dijet azimuthal angular distributions to determine the J^{PC} quantum number of the diphoton resonance. Constraints on the parameter space can be obtained by interpreting some of the small diphoton "excesses" reported by the LHC as the composite scalar or pseudoscalar of the model. Another important test of the model is the presence of a nearby hypercolor-singlet but color-octet state like the $^1S_0$ state η_Q^8 or $\eta_{\tilde{Q}}^8$, which can also be constrained by dijet or monojet plus monophoton data. Both possibilities of a large or small width of the resonance can be accommodated, depending on whether the hyper-glueball states are kinematically allowed in the final state or not.

DOI: 10.1103/PhysRevD.95.115034

I. INTRODUCTION

It is well known that the discovery mode of the 125 GeV Standard Model (SM) Higgs boson at the Large Hadron Collider (LHC) is the diphoton channel, $h_{\rm SM}(125\ {\rm GeV}) \to \gamma\gamma$. Perhaps it is somewhat ironic that the discovery mode of the Higgs boson has something to do with the one-loop induced higher-dimension operator[1] for the diphoton mode, rather than the other renormalizable tree-level vertices coming from the spontaneous breaking of the electroweak gauge symmetry via the Higgs mechanism. All such tree-level couplings, $hf\bar{f}$ and hVV (f and V denote the SM fermion and the weak gauge boson, respectively), are proportional to the masses of the final-state particles, which is a generic feature of the Higgs mechanism. Thus, for a relatively light SM Higgs of 125 GeV, all kinematically accessible tree-level processes are suppressed by the light masses of the final-state particles. It is therefore of the utmost importance for LHC run II (as well as for future e^+e^- colliders like CEPC or ILC) to verify that the 125 GeV boson does couple to the SM fermions and that weak gauge bosons are in line with SM expectations.

Nevertheless, the diphoton mode remains an important process, since it is a very clean signal at the LHC. In particular, this mode may play a role for probing new physics beyond the SM. Recall that the 750 GeV bump reported around Christmas time in 2015 by the two LHC collaborations [1,2] is also a diphoton resonance. This bump was very hard to explain within SM, and many different ideas have been proposed to accommodate this. Unfortunately, it was rather short lived—the "excess" has faded away in the summer after more data were collected and analyzed [3,4].

[*]pko@kias.re.kr
[†]chyu@korea.ac.kr
[‡]tcyuan@gate.sinica.edu.tw

[1]The dominant production mechanism for the SM Higgs at the LHC is also a one-loop induced gluon fusion process.

It is not necessary for diphoton resonance to arise from one-loop induced amplitude. An attractive alternative scenario is to introduce a composite bound state of new heavy particles with QCD and/or QCD-like interactions, as was considered in Refs. [5–13] to explain the "excess" of the 750 GeV bump. Here the diphoton amplitude is not suppressed by the loop but rather by the wave function for finding two heavy particles at the origin to form the bound state. This scenario is distinguishable from another interesting scenario, where the diphoton excess is due to a pseudo–Nambu-Goldstone boson (pNGB) coming from the spontaneous breakdown of a global symmetry [14–24], and the diphoton amplitude is suppressed by the anomaly term. In general, the new composite states can be investigated through any diboson resonance as well as diphoton resonance at the LHC [25–32].

In this paper, we explore in detail such a scenario in which diphoton (or in general, diboson) resonance that might appear in the future LHC experiments may be due to new confining strong interaction (which we call hypercolor interaction, or h-QCD in short) and new particles (h-quark Q or scalar h-quark $\tilde{Q}$) that feel not only this new strong force but also the SM gauge interactions. If the new particles belong to a $SU(2)_L$ doublet and feel strong color interactions, it would modify the 125 GeV Higgs signal strength in the $gg \to H \to \gamma\gamma$ channel. And there would be strong constraints from electroweak precision tests parametrized by the oblique S and T parameters. To avoid these issues, we assume that the new particles are colored but $SU(2)_L$ singlets with hypercharge $Y = e_Q$.[2] We consider the spin of the new particle being either 0 (complex scalar boson $\tilde{Q}$) or 1/2 (Dirac fermion Q) and study their lowest-lying bound states, $\eta_{\tilde{Q}}(^1S_0)$, $\eta_Q(^1S_0)$, and $\psi_Q(^3S_1)$.

For the case where the new fermion Q belongs to a $SU(2)_L$ doublet but feels no strong color interaction, as was discussed previously in the context of quirks [33] or iquarks [34], besides the $\gamma\gamma$, ZZ, and $Z\gamma$ channels, other diboson decay modes of the hyperquarkonia like W^+W^-, $W^\pm\gamma$, and $W^\pm Z$ in the final states are also possible. A more general case for the heavy fermion Q being a colored $SU(2)_L$ doublet will be treated in Ref. [35].

The paper is structured as follows: In Sec. II, we set up the model of hypercolor QCD and discuss its bound-state spectra, including the $^1S_0$ color-octet states η_Q^8 and $\eta_{\tilde{Q}}^8$. The productions and decays of the bound states at the LHC for the vectorlike hyperquark and the scalar hyperquark cases are discussed in Secs. III and IV, respectively. In Sec. V, we briefly discuss how to distinguish between the two scenarios of hyperquark and hyperscalar quark composites. In Sec. VI, we discuss the possible interpretation of the high-mass diphoton resonances at 710 GeV and 1.6 TeV reported with small "excesses" at the LHC as a composite scalar $\eta_{\tilde{Q}}$ or pseudoscalar η_Q in the model. We also briefly discuss the small "excess" of the photon + jet resonance at 2 TeV as the decay product of the color-octet state η_Q^8 or $\eta_{\tilde{Q}}^8$. Finally, we summarize our study in Sec. VII.

II. HYPERCOLOR MODEL SETUP

For the hyper–strongly interacting model, we assume that

(1) There is a new confining gauge group $SU(N_h)$ with strong coupling g' and a confinement scale Λ_h, defined as

$$\Lambda_h \simeq M \exp\left[-\frac{6\pi}{(11N_h - 2n_{f^h})\alpha_h(M)}\right], \quad (1)$$

where n_{f^h} is the number of hyperquark flavors, M is a heavy mass scale, and $\alpha_h = g'^2/4\pi$.

(2) There is a new vectorlike h-quark (hyperquark) Q and its antiparticle $\bar{Q}$ (or scalar h-quark $\tilde{Q}$ and its antiparticle $\tilde{Q}^\dagger$), whose quantum numbers under the $SU(3)_C \times SU(2)_L \times U(1)_Y \times SU(N_h)$ are defined as $(3, 1, Y; N_h)$.

(3) Both Q and $\tilde{Q}$ are heavier than the confinement scale Λ_h, so that $Q\bar{Q}$ ($\tilde{Q}\tilde{Q}^\dagger$) bound states can be treated as heavy hyperquarkonia, analogous to J/ψ, η_c, Υ, η_b, etc. in QCD.

If $\alpha_h(m_Q v_Q)m_Q > \Lambda_h$, the bound system would be more like a Coulombic bound state, since the nonperturbative confinement effect would be smaller than the Coulomb interaction. One can show that Coulomb dominance can be a reasonably good approximation for the entire range of α_h [35]. In the following, we will accept this assumption and present various numerical results assuming the binding potential V is Coulombic. Namely,

$$V = -\frac{C_h\alpha_h}{r} - \frac{C_F\alpha_s}{r}, \quad (2)$$

with $C_h = (N_h^2 - 1)/(2N_h)$ and $C_F = (N_c^2 - 1)/(2N_c)$. Note that the new strong interaction dominates over QCD interaction for $\alpha_h(M) \gtrsim 0.2$, while the two interactions are competitive with each other for $\alpha_h(M) \sim 0.1$. When interpreting the results, one has to keep in mind that these numerical results are based on the assumption of Coulomb dominance. The wave function at the origin for the radial quantum number $n = 1$ S-wave ground state assuming Coulomb dominance is given by [36]

$$|R_{1S}(0)|^2 = m_Q\left\langle\frac{dV}{dr}\right\rangle = 4\left([C_h\alpha_h + C_F\alpha_s]\frac{m_Q}{2}\right)^3. \quad (3)$$

This nonperturbative quantity is very important, since it determines both production and decay rates of the S-wave

[2]In the numerical analysis, we will take $Y = e_Q = 2/3$, and one can easily scale the results for other values of $Y = e_Q$.

$Q\bar{Q}$ bound states. The wave function $\tilde{R}_{1S}(0)$ for the $\tilde{Q}\tilde{Q}^\dagger$ bound state is approximately the same as $R_{1S}(0)$, up to the one-loop correction to the hyper-QCD potential [37].

Besides the heavy Q, there is also the massless h-gluon g_h. Due to h-color confinement, the lightest h-hadron would be a scalar or pseudoscalar h-glueball state. For pure $SU(3)_h$ case, the lightest scalar glueball mass is given by $m_0 \sim (4\text{–}7)\Lambda_h$ [38–40]. Depending on the mass of the h-glueball, the lightest $Q\bar{Q}$ (or $\tilde{Q}\tilde{Q}^\dagger$) bound state may or may not decay into two h-glueballs. In this work, we consider cases where decay into h-glueballs is either open or forbidden kinematically.

A. Spectra of new resonances

We assume that $\alpha_h(m_Q v_Q) \sim v_Q^2 \ll 1$, so that the h-QCD version of nonrelativistic QCD (NRQCD) [41] for charmonia and bottomonia applies. Otherwise, there is no systematic way to calculate decay and production rates for the bound states. This condition implies that if $\alpha_h(M) \sim 0.5$ or larger, then the system would no longer be nonrelativistic, and there is no guarantee that the NRQCD approach would give a good description of $Q\bar{Q}$ bound states. As mentioned before, we also assume $\alpha_h M \gg \Lambda_h$, so that the nonperturbative effects are small and one can make an approximation using the Coulomb potential for the $Q\bar{Q}$ system. Then the binding energy of this system is approximately given by

$$M(n^{2S+1}L_J) \simeq 2m_Q\left[1-\frac{(C_h\alpha_h+C_F\alpha_s)^2}{8n^2}\right]. \quad (4)$$

Note that the degeneracy in the orbital quantum number l is special only for the Coulomb potential. The mass of the lowest state, η_Q, is approximately given by $M_{\eta_Q} = M(1^1S_0) \approx 2m_Q$ for small α_h. The excited 2^1S_0 state η_Q' has a mass

$$M(\eta_Q') = 2m_Q\left(\frac{1-[C_h\alpha_h+C_F\alpha_s]^2/32}{1-[C_h\alpha_h+C_F\alpha_s]^2/8}\right). \quad (5)$$

For instance, for $\alpha_h = 0.2$ and $m_Q = 1$ TeV, the mass difference of η_Q' and η_Q is about 28, 47, and 70 GeV for $N_h = 3$, 4, and 5, respectively.

The mass of a spin-triplet partner ψ_Q is determined by hyperfine splitting

$$\frac{M_{\psi_Q}-M_{\eta_Q}}{M_{\eta_Q}} = \frac{16\pi}{3}\alpha_h\frac{|R_S(0)|^2}{M^3} \approx \frac{\pi}{3n^2}(C_h\alpha_h+C_F\alpha_s)^4, \quad (6)$$

where the last equation only holds for Coulomb potential between Q and $\bar{Q}$. The resulting mass splitting between $^1S_0$ and $^3S_1$ is

$$\Delta M \lesssim (45, 122, 264)\ \text{GeV for } N_h = (3,4,5). \quad (7)$$

For simplicity, we ignore the mass difference and set $M_{\psi_Q} = M_{\eta_Q}$ in our analysis.

In the scalar h-quark scenario, we expect that the mass spectrum of low-lying states is the same as that in the h-quark case up to one-loop correction and spin-dependent hyperfine splitting,[3] because the potentials in the two scenarios are identical.

B. Color-octet bound state

Next, we consider the $Q\bar{Q}(^1S_0)$ bound state, η_Q^8, which is a singlet under h-QCD, but an octet under ordinary QCD. One can easily extend the analysis to other color-octet states with different spin and orbital angular momentum. It is well known that the potential of a $Q\bar{Q}$ pair is attractive in the color-singlet state, but repulsive in the color-octet state. Nevertheless, the η_Q^8 bound state can still be formed because the attractive hyper–strong interaction is stronger than the repulsive one from ordinary QCD. The potential of the $Q\bar{Q}$ pair is expressed as the sum of two terms

$$V = -\frac{C_h\alpha_h}{r}+\frac{C_8\alpha_s}{r}, \quad (8)$$

where $C_8 = C_A/2 - C_F$ with $C_A = N_c$. The wave function $R^8_{\eta_Q}(0)$ at the origin of η_Q^8 can be given in the same form as Eq. (3) by the substitution of $C_h\alpha_h + C_F\alpha_s \to C_h\alpha_h - C_8\alpha_s$.

Similarly, one can obtain the wave function at the origin, $\tilde{R}^8_{\eta_{\tilde{Q}}}(0)$, for the scalar h-quark pair.

III. BOUND STATES OF HYPERQUARKS

In this section, we consider a vectorlike h-quark singlet Q with $Y = e_Q = 2/3$ and mass m_Q. Q belongs to the fundamental representations of both $SU(N_h)$ and ordinary $SU(3)_C$ gauge theories, and thus feels new strong interaction as well as ordinary strong interaction. First, we consider the spin-singlet S-wave state $\eta_Q(^1S_0)$. Then, the spin-triplet S-wave state $\psi_Q(^3S_1)$ will be taken into account.

A. Production and decay of η_Q

The pseudoscalar bound state η_Q of new hidden quarks can decay into two photons, γZ, ZZ, two gluons, or two h-gluons. Their decay widths are given by

$$\Gamma(\eta_Q \to \gamma\gamma) = \frac{N_c N_h \alpha^2 e_Q^4}{m_Q^2}|R_{1S}(0)|^2, \quad (9)$$

[3]The hyperfine splitting is proportional to $1/m_Q^2$, so that it would be negligible for heavy h-quarks.

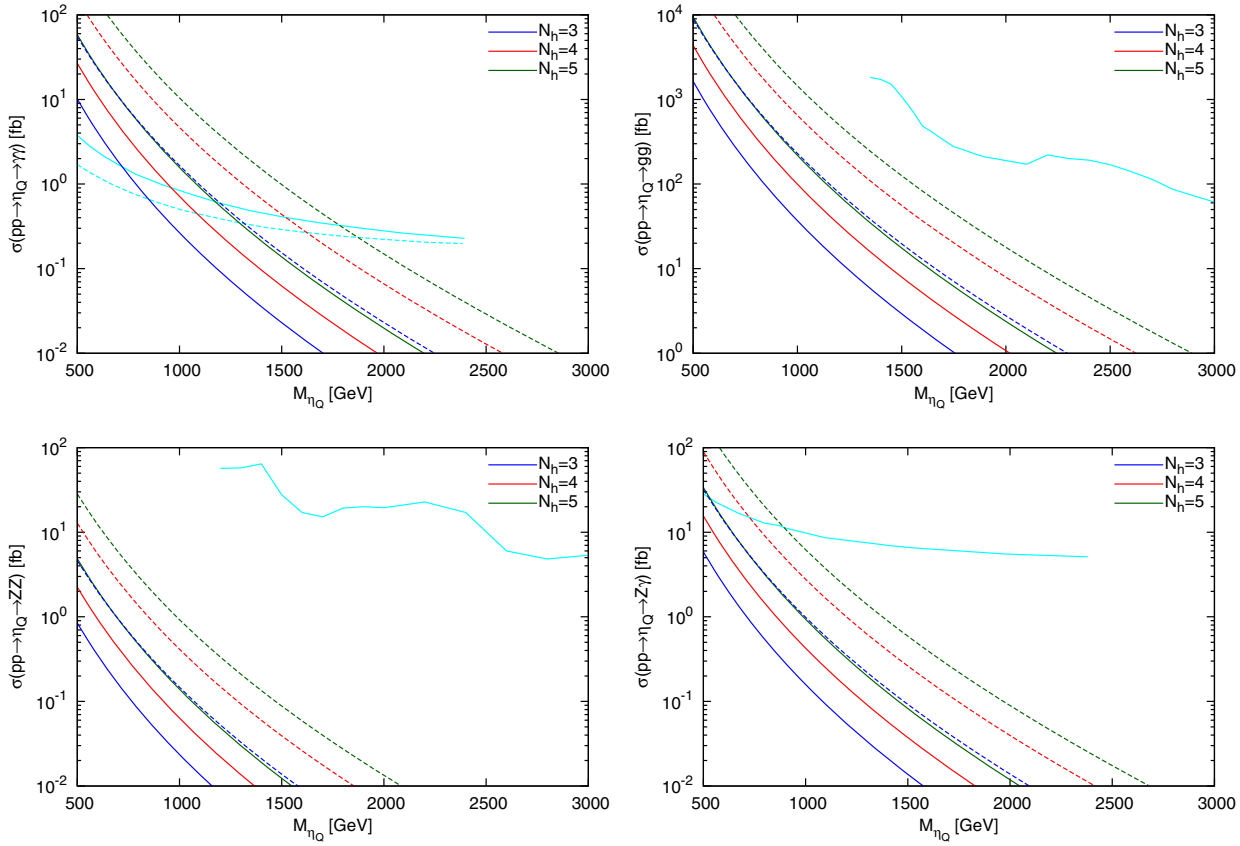

FIG. 1. The cross sections for (a) $pp \to \eta_Q \to \gamma\gamma$, (b) $pp \to \eta_Q \to gg$, (c) $pp \to \eta_Q \to ZZ$, and (d) $pp \to \eta_Q \to Z\gamma$ for $\alpha_h = 0.2$ at the LHC with $\sqrt{s} = 13$ TeV in units of fb as functions of M_{η_Q}. The blue, red, and green solid (dashed) lines in these plots correspond to the $N_h = 3$, 4, and 5 cases, respectively, in which $\eta_Q \to g_h g_h$ is allowed (forbidden). See the text for explanation of the cyan lines in each of these plots.

$$\Gamma(\eta_Q \to gg) = \frac{C_F N_h \alpha_s^2}{2m_Q^2} |R_{1S}(0)|^2, \tag{10}$$

$$\Gamma(\eta_Q \to \gamma Z) = (x_w(4 - r_Z)/2(1 - x_w))\Gamma(\eta_Q \to \gamma\gamma), \tag{11}$$

$$\Gamma(\eta_Q \to ZZ) = \frac{4N_c N_h \alpha^2 e_Q^4 x_w^2 (1 - r_Z)^{3/2}}{m_Q^2 (2 - r_Z)^2 (1 - x_w)^2} |R_{1S}(0)|^2, \tag{12}$$

$$\Gamma(\eta_Q \to g_h g_h) = (C_h N_c \alpha_h^2 / C_F N_h \alpha_s^2)\Gamma(\eta_Q \to gg). \tag{13}$$

Here $x_w = \sin^2\theta_W$ and $r_Z = m_Z^2/4m_Q^2$. We note that η_Q does not decay into a pair of fermions or WW owing to the singlet nature of Q and the J^{PC} quantum number of η_Q being 0^{-+}.[4] The branching ratios strongly depend on α_h if $\eta_Q \to g_h g_h$ is allowed. For $\alpha_h \sim 0.1$, $\mathrm{BR}(\eta_Q \to g_h g_h) \sim \mathrm{BR}(\eta_Q \to gg) \sim 0.5$. However, for $\alpha_h \gtrsim 0.2$, the $\eta_Q \to g_h g_h$ channel is dominant. If $\eta_Q \to g_h g_h$ is kinematically forbidden, $\mathrm{BR}(\eta_Q \to gg)$ becomes 0.99 irrespective of α_h and N_h [35].

At the LHC, the η_Q can be produced via gluon fusion. The cross section for the diphoton production $pp \to \eta_Q \to \gamma\gamma$ is given by

$$\sigma(pp \to \eta_Q \to \gamma\gamma) = \frac{C_{gg}}{sM_{\eta_Q}\Gamma_{\mathrm{tot}}}\Gamma(\eta_Q \to gg)\Gamma(\eta_Q \to \gamma\gamma), \tag{14}$$

where C_{gg} is defined as [42]

$$C_{gg} = \frac{\pi^2}{8}\int_{M^2/s}^1 \frac{d\tau}{\tau} f_g(\tau) f_g(M^2/s\tau), \tag{15}$$

with $f_g(\tau)$ being the gluonic parton distribution function at the longitudinal momentum fraction of the gluon τ. By making use of the MSTW2008NLO data at $\sqrt{s} = 13$ TeV [43], one finds that $C_{gg} = 2137$ and 7.14 at $M = 750$ and 2 TeV, respectively. Similarly, one can obtain the cross section for the two-gluon production via the η_Q decays.

[4]We shall ignore loop-induced decays such as $\eta_Q \to \gamma^*\gamma^*$, Z^*Z^*, $Z^*\gamma^* \to f\bar{f}$, W^+W^-, because they are loop suppressed.

In Fig. 1, we show the production cross sections of (a) two photons, (b) two gluons, (c) two Z bosons, and (d) $Z\gamma$ via the η_Q resonance for $\alpha_h = 0.2$ as functions of the mass of η_Q, M_{η_Q}. The blue, red, and green lines denote the $N_h = 3$, 4, and 5 cases, respectively, where the solid (dashed) lines correspond to the cases in which the $\eta_Q \to g_h g_h$ channel is open (closed).

In Fig. 1(a), the solid (dashed) cyan line represents the expected 95% C.L. upper limit on the fiducial cross section times the branching ratio of a spin-0 resonance to two photons at $\sqrt{s} = 13$ TeV in ATLAS data by assuming the ratio $\Gamma/M_{\eta_Q} = 2\%$ ($\Gamma = 4$ MeV) [3]. We note that the observed 95% C.L. upper limit in ATLAS is almost the same as the one expected by the ATLAS Collaboration [3]. Since the total decay width of η_Q is about 150 MeV to 10 GeV for $\alpha_h = 0.2$, one could impose the bound on the model somewhere between the two cyan lines. Note that the ratio Γ/M_{η_Q} could be about 10% for larger α_h. As shown in Fig. 1(a), the lower bound on M_{η_Q} is about 800 (1200) GeV for $N_h = 3$ (5) if $\eta_Q \to g_h g_h$ is allowed, while it could be about 1300 (1900) GeV if $\eta_Q \to g_h g_h$ is closed. The difference for the lower bounds simply arises from the difference in the total decay width of η_Q, which is much larger in the former case.

In Figs. 1(b)–1(d), we show the cross sections for (b) $pp \to \eta_Q \to gg$, (c) $pp \to \eta_Q \to ZZ$, and (d) $pp \to \eta_Q \to Z\gamma$. The cyan lines denote the observed 95% C.L. upper limits on the fiducial cross section times branching ratio for (b) dijet production [44], (c) ZZ production [45], and (d) $Z\gamma$ production [46] at $\sqrt{s} =$ 13 TeV in ATLAS data. As shown in Fig. 1, the gg and ZZ productions are not constrained by experiments yet. However, the search for a resonance which decays into $Z\gamma$ starts by constraining this model, in particular, in the case that $\eta_Q \to g_h g_h$ is forbidden.

In summary, the case of $pp \to \eta_Q \to \gamma\gamma$ is mostly constrained by current experimental data. In other words, $\eta_Q \to \gamma\gamma$ would be the most promising channel for probing this composite model. One may obtain similar results with experimental bounds at $\sqrt{s} = 8$ or 13 TeV in CMS or ATLAS for $pp \to \gamma\gamma$ [47–49], $pp \to jj$ [50–54], $pp \to ZZ$ [55–65], and $pp \to Z\gamma$ [66–70].

B. Production and decay of ψ_Q

One of the decisive tests for a spin-singlet S-wave bound state η_Q of a new fermion-antifermion pair would be to search for its spin-triplet partner ψ_Q which is almost degenerate with η_Q. This state is analogous to J/ψ in the charmonia and has $J^{PC} = 1^{--}$. Here, we discuss the decay and production of a color-singlet spin-triplet ψ_Q. Due to its quantum numbers, ψ_Q does not decay into two gluons and two h-gluons. It can decay into ggg, $g_h g_h g_h$, $gg\gamma$, $g_h g_h \gamma$, or a pair of fermions via a virtual photon or Z boson. Because of the singlet nature of Q and $J^{PC} = 1^{--}$, ψ_Q does not decay into two EW gauge bosons if the $SU(2)_L \times U(1)_Y$ gauge symmetry remains unbroken. We find that ψ_Q can decay into WW due to small effects of EW symmetry breaking, but the branching ratio of $\psi_Q \to WW$ is quite small.

The decay rates of the ψ_Q into the ggg and l^+l^- ($l = e, \mu, \tau$) final states are given by

$$\Gamma(\psi_Q \to ggg) = \frac{(\pi^2 - 9)\alpha_s^3}{36\pi m_Q^2} \frac{N_h (N_c^2 - 1)(N_c^2 - 4)}{N_c^2} |R_{1S}(0)|^2, \tag{16}$$

$$\Gamma(\psi_Q \to l^+l^-) = \frac{N_c N_h \alpha^2 e_Q^2}{3m_Q^2} \left[1 - \frac{2(1 - 4x_w)}{(4 - r_Z)(1 - x_w)} + \frac{2(1 - 4x_w + 8x_w^2)}{(4 - r_Z)^2 (1 - x_w)^2}\right] |R_{1S}(0)|^2. \tag{17}$$

The decay rate for $\psi_Q \to g_h g_h g_h$ is given by Eq. (16) by replacing α_s, N_h, and N_c with α_h, N_c, and N_h, respectively. We consider cases in which this decay channel is allowed or kinematically closed. Note that $\psi_Q \to g_h g_h \gamma$ is also possible if the mass of the scalar h-glueball is less than M_{ψ_Q}. The decay rates for other channels will be presented in Ref. [35]. The branching ratios for ψ_Q strongly depend on α_h, and $\psi_Q \to g_h g_h g_h$ or $g_h g_h \gamma$ becomes a dominant decay channel for $\alpha_h \gtrsim 0.2$–0.3. However, for $\alpha_h \sim 0.1$, $\psi_Q \to l^+l^-$ is dominant, and its branching ratio is about 0.3 [35]. Therefore, the dilepton production via the ψ_Q resonance would be another promising channel for probing or constraining this model for smaller α_h. We also note that the search for a new resonance in dijet events can constrain this model via $pp \to \psi_Q \to q\bar{q}$.

As is well known, the ψ_Q resonance is strongly constrained by the Drell-Yan (DY) production of $q\bar{q} \to \psi_Q \to l^+l^-$ in pp collisions with the following cross section:

$$\sigma_{\rm DY}(pp \to \psi_Q \to l^+l^-) = \frac{(2J_{\psi_Q} + 1)\Gamma(\psi_Q \to l^+l^-)}{sM_{\psi_Q}\Gamma_{\psi_Q}} \times \sum_{q\bar{q}} C_{q\bar{q}} \Gamma(\psi_Q \to q\bar{q}), \tag{18}$$

where $C_{q\bar{q}}$ is given by [42]

$$C_{q\bar{q}} = \frac{4\pi^2}{9} \int_{M^2/s}^1 \frac{d\tau}{\tau} [f_q(\tau) f_{\bar{q}}(M^2/s\tau) + f_{\bar{q}}(\tau) f_q(M^2/s\tau)]. \tag{19}$$

Here, $f_{q,\bar{q}}$ denote the parton distribution functions of q and $\bar{q}$ evaluated at the scale $\mu = M_{\psi_Q}$, and $J_{\psi_Q} = 1$ is the spin of ψ_Q. For example, by making use of the

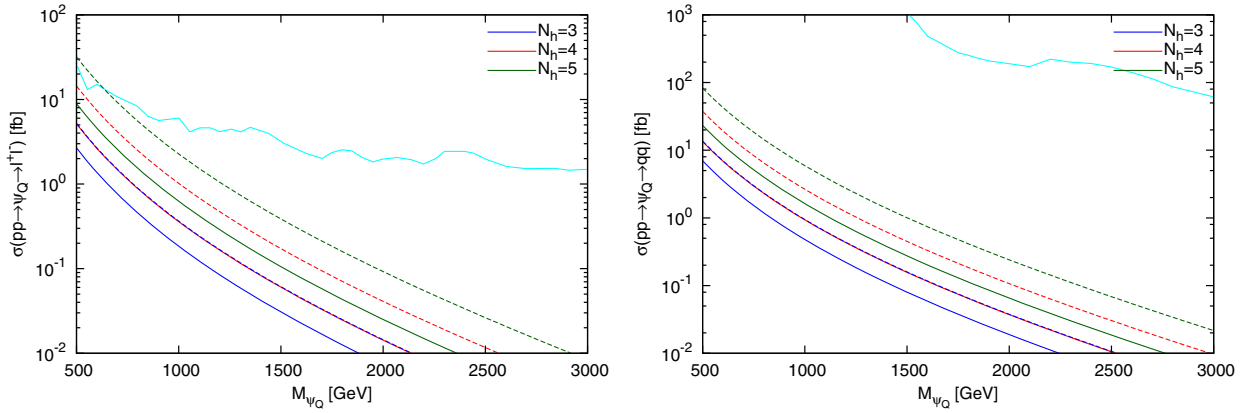

FIG. 2. The cross sections for (a) $pp \to \psi_Q \to l^+l^-$ and (b) $pp \to \psi_Q \to q\bar{q}$ in units of fb for $\alpha_h = 0.2$ as functions of M_{ψ_Q} at the LHC with $\sqrt{s} = 13$ TeV. The solid (dashed) lines correspond to the case in which $\psi_Q \to g_h g_h g_h$ is allowed (forbidden). See the text for explanation of the cyan lines.

MSTW2008NLO data [43], at $\sqrt{s} = 13$ TeV, one obtains $C_{u\bar{u}} = 1054$, $C_{d\bar{d}} = 627$, $C_{s\bar{s}} = 83$, $C_{c\bar{c}} = 36$, and $C_{b\bar{b}} = 15.3$ for $\mu = 750$ GeV; and $C_{u\bar{u}} = 14.9$, $C_{d\bar{d}} = 7.1$, $C_{s\bar{s}} = 0.33$, $C_{c\bar{c}} = 0.11$, and $C_{b\bar{b}} = 0.044$ for $\mu = 2$ TeV. In dijet production, $\Gamma(\psi_Q \to l^+l^-)$ is replaced by $\sum \Gamma(\psi_Q \to q\bar{q})$ in Eq. (18).

In Fig. 2(a), the cross section for the DY process, $pp \to \psi_Q \to l^+l^-$ ($l =$ either e or μ), for $\alpha_h = 0.2$ at $\sqrt{s} = 13$ TeV is shown in solid (dashed) lines in the case in which $\psi_Q \to g_h g_h g_h$ is allowed (forbidden). The cyan line denotes the upper 95% C.L. limit on the cross section times the branching ratio to two leptons at $\sqrt{s} = 13$ TeV in ATLAS data [71]. As shown in Fig. 2(a), the ψ_Q production is not constrained by the DY process except in the region in which $M_{\psi_Q} \lesssim 700$ GeV and $N_h = 5$ when $\psi_Q \to g_h g_h g_h$ is forbidden.

In Fig. 2(b), we show the dijet production cross section in $pp \to \psi_Q \to q\bar{q}$ at $\sqrt{s} = 13$ TeV. The cyan line corresponds to the same upper bound as in Fig. 1(a) with the lepton pair's branching ratio replaced by the light quark pair's branching ratio. The search for a new resonance in the dijet production does not constrain this model yet.

C. Excited states

Another characteristic feature of any composite model is the existence of excited states, similar to ψ', η_c', $\Upsilon(nS)$, and so on. These excited states can cascade-decay into the ground state(s) by emitting h-gluons, gluons, and electroweak gauge bosons, in analogy with $\psi' \to J/\psi\pi\pi$, $\eta_c\gamma$, etc. All these channels require detailed information on the bound-state spectra and the wave functions, and we will not consider them any further in this paper.

In passing, we briefly mention the decays and the productions of an excited state η_Q', which is the 2^1S_0 state. We find that the cross section for $pp \to \eta_Q' \to \gamma\gamma$ could be about 12% of that for $pp \to \eta_Q \to \gamma\gamma$.

D. Production and decay of the color-octet bound state

In this section, we consider the production and decay of the color-octet bound state, η_Q^8, which could be formed when the h-color-singlet interaction of $Q\bar{Q}$ is much stronger than the color-octet QCD interaction.

η_Q^8 can decay into two-body modes gg, $g\gamma$, Zg and three-body modes ggg, $gg\gamma$, as well as gg_hg_h (if kinematically allowed). Note that it does not decay into $\gamma\gamma$ or g_hg_h due to color conservation. Also, $\eta_Q^8 \to g\gamma$ is the unique signature for the color-octet bound state, unlike the usual color-singlet bound states. The final state $\gamma +$ jet is the same as the final state of the excited quark decay $q^* \to q\gamma$, so the bounds from the excited quark searches would apply here. The three-body modes are suppressed by phase space and will be treated elsewhere [35]. The decay rates of $\eta_Q^8 \to gg$, γg, and Zg are

$$\Gamma[\eta_Q^8 \to gg] = \frac{(N_c^2-1)(N_c^2-4)N_h\alpha_s^2}{64N_c m_Q^2}|R_{\eta_Q}^8(0)|^2, \quad (20)$$

$$\Gamma[\eta_Q^8 \to \gamma g] = \frac{(N_c^2-1)N_h\alpha_s\alpha e_Q^2}{8m_Q^2}|R_{\eta_Q}^8(0)|^2, \quad (21)$$

$$\Gamma[\eta_Q^8 \to Zg] = \frac{(N_c^2-1)N_h\alpha_s\alpha e_Q^2 x_w(4-r_Z)}{32(1-x_w)m_Q^2}|R_{\eta_Q}^8(0)|^2. \quad (22)$$

The branching ratios in each of the above decay channels are 0.70, 0.15, and 0.15, respectively.

The production of the color-octet bound state can be constrained by resonance searches in the dijet production corresponding to the $pp \to \eta_Q^8 \to gg$ mode, and in the $\gamma +$ jet production corresponding to the $pp \to \eta_Q^8 \to \gamma g$ mode. In Fig. 3, we depict the cross sections for Fig. 3(a) $pp \to \eta_Q^8 \to \gamma g$ and Fig. 3(b) $pp \to \eta_Q^8 \to gg$ by setting

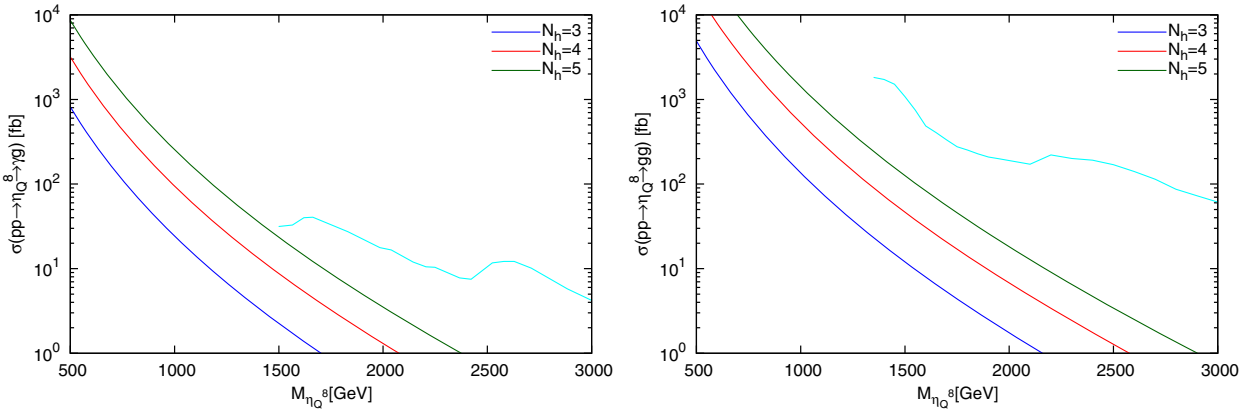

FIG. 3. The cross sections for (a) $pp \to \eta_Q^8 \to \gamma g$ and (b) $pp \to \eta_Q^8 \to gg$ in units of fb for $\alpha_h = 0.2$ as functions of $M_{\eta_Q^8}$ at the LHC with $\sqrt{s} = 13$ TeV. See the text for explanation of the cyan lines.

$\alpha_h = 0.2$ as functions of $M_{\eta_Q^8}$. The cyan line in Fig. 3(a) denotes the 95% C.L. limit on the production cross section times the branching ratio to a photon and a quark or a gluon for an excited quark q^* at $\sqrt{s} = 13$ TeV in ATLAS data [72]. Similar limits can be obtained from the bounds for the excited quark production at $\sqrt{s} = 8$ or 13 TeV in CMS or ATLAS data [73–76]. The cyan line in Fig. 3(b) is the same as that in Fig. 1(b). As shown clearly in Fig. 3, both production modes at $\sqrt{s} = 13$ TeV do not constrain this model for $\alpha_h = 0.2$. However, for larger α_h, this model would be constrained, in particular, in the γg production channel.

IV. BOUND STATES OF SCALAR HYPERQUARKS

In this section, we consider extra scalar quark singlet $\tilde{Q}$ with $Y = e_Q = 2/3$ and mass $m_{\tilde{Q}}$. $\tilde{Q}$ belongs to the fundamental representation of $SU(N_h)$ gauge theory like Q. The lowest bound state is denoted as $\eta_{\tilde{Q}}$, which is a color as well as a hypercolor singlet bound state of $\tilde{Q}\tilde{Q}^\dagger$ in the S-wave state $\eta_{\tilde{Q}}(^1S_0)$ with $J^{PC} = 0^{++}$. There will be no analogy of ψ_Q $(^3S_1)$ if the constituent particles are scalar quarks rather than Dirac fermions. Instead, the $J^{PC} = 1^{--}$ state $(\chi_{\tilde{Q}})$ arises from higher radial excitation with nonzero orbital angular momentum, $J = L = 1$. Since the vector resonance for scalar constituents has a zero node at the origin in the radial wave function, the wave function vanishes there. Its production rate will be suppressed by the derivative of the wave function, and thus it will be relatively smaller than the S-wave ground state.

A. Productions and decays of $\eta_{\tilde{Q}}$, $\chi_{\tilde{Q}}$, and $\eta_{\tilde{Q}}^8$

The scalar bound state $\eta_{\tilde{Q}}$ of new scalar h-quarks can decay into two photons, γZ, ZZ, two gluons, or two h-gluons. The decay widths of these modes are given by

$$\Gamma(\eta_{\tilde{Q}} \to \gamma\gamma) = \frac{N_c N_h \alpha^2 e_Q^4}{2m_Q^2} |\tilde{R}_{1S}(0)|^2, \tag{23}$$

$$\Gamma(\eta_{\tilde{Q}} \to \gamma Z) = \frac{N_c N_h \alpha^2 e_Q^4 x_w (4 - r_Z)}{4m_Q^2 (1 - x_w)^2} |\tilde{R}_{1S}(0)|^2, \tag{24}$$

$$\Gamma(\eta_{\tilde{Q}} \to ZZ) = \frac{N_c N_h \alpha^2 e_Q^4 x_w^2 (8 - 8r_Z + 3r_Z^2)\sqrt{1 - r_Z}}{4m_Q^2 (2 - r_Z)^2 (1 - x_w)^2} |\tilde{R}_{1S}(0)|^2, \tag{25}$$

$$\Gamma(\eta_{\tilde{Q}} \to gg) = \frac{N_h (N_c^2 - 1)\alpha_s^2}{8N_c m_Q^2} |\tilde{R}_{1S}(0)|^2, \tag{26}$$

$$\Gamma(\eta_{\tilde{Q}} \to g_h g_h) = \frac{N_c (N_h^2 - 1)\alpha_h^2}{8N_h m_Q^2} |\tilde{R}_{1S}(0)|^2, \tag{27}$$

where $\tilde{R}_{1S}(0)$ is the wave function at the origin of the scalar quark bound state. Note that $\tilde{R}_{1S}(0)$ is the same as $R_{1S}(0)$ up to one-loop-order correction for the QCD-like potential [37] and the hyperfine splitting, which is absent in the case of the scalar h-quark. We note that $\eta_{\tilde{Q}}$ does not decay into a pair of fermions or WW, just like the case of η_Q.

The branching ratios strongly depend on α_h if $\eta_{\tilde{Q}} \to g_h g_h$ is allowed. For $\alpha_h \sim \alpha_s$ and $N_h = 3$, both $\mathrm{BR}(\eta_{\tilde{Q}} \to g_h g_h)$ and $\mathrm{BR}(\eta_{\tilde{Q}} \to gg)$ approach 0.5. However, for $\alpha_h \gtrsim 0.2$, $\mathrm{BR}(\eta_{\tilde{Q}} \to g_h g_h)$ becomes dominant over other decay channels. Actually, $\mathrm{BR}(\eta_{\tilde{Q}} \to g_h g_h) \gtrsim 0.8$ for $\alpha_h = 0.2$ [35]. On the other hand, if $\eta_{\tilde{Q}} \to g_h g_h$ is kinematically closed, $\mathrm{BR}(\eta_{\tilde{Q}} \to gg)$ becomes more than 0.98 in the entire parameter space.

In Figs. 4(a)–4(d), we plot the cross sections for $pp \to \eta_{\tilde{Q}} \to \gamma\gamma$, $pp \to \eta_{\tilde{Q}} \to gg$, $pp \to \eta_{\tilde{Q}} \to ZZ$, and (d) $pp \to \eta_{\tilde{Q}} \to Z\gamma$, respectively, for $\alpha_h = 0.2$ at

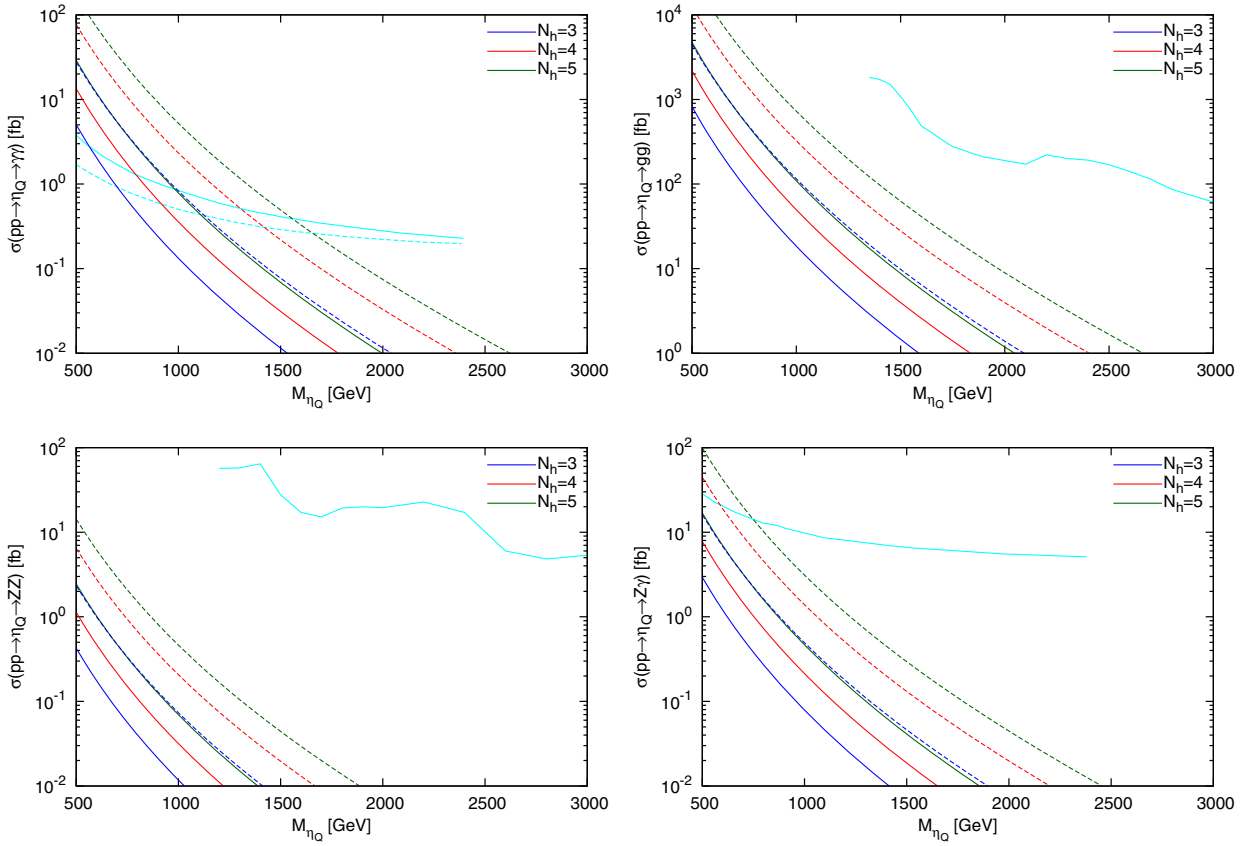

FIG. 4. The cross sections for (a) $pp \to \eta_{\tilde{Q}} \to \gamma\gamma$, (b) $pp \to \eta_{\tilde{Q}} \to gg$, (c) $pp \to \eta_{\tilde{Q}} \to ZZ$, and (d) $pp \to \eta_{\tilde{Q}} \to Z\gamma$ for $\alpha_h = 0.2$ at the LHC with $\sqrt{s} = 13$ TeV in units of fb as functions of $M_{\eta_{\tilde{Q}}}$. The cyan lines are the same experimental upper bounds as in Fig. 1.

$\sqrt{s} = 13$ TeV, as functions of $M_{\eta_{\tilde{Q}}}$ with the same experimental upper bounds as in Fig. 1. The solid (dashed) lines correspond to the cases in which the $\eta_{\tilde{Q}} \to g_h g_h$ decay is allowed (forbidden). The cross sections for the $\eta_{\tilde{Q}}$ production in Fig. 4 are a little bit smaller than those for the η_Q production in Fig. 1. The difference mainly originates in the different spins of the particles constituting the bound states. However, general features are the same as in Fig. 1.

The vector resonance $\chi_{\tilde{Q}}$ can decay into a pair of leptons, and thus it is constrained by the DY process like ψ_Q in the fermion case. We find that the production cross section for $pp \to \chi_{\tilde{Q}} \to l^+ l^-$ is highly suppressed by the derivative of the wave function at the origin. For $M_{\eta_{\tilde{Q}}} > 500$ GeV, we find that $\sigma(pp \to \chi_{\tilde{Q}} \to l^+ l^-) \lesssim O(10^{-4})$ fb, which is much smaller than the LHC upper bound. Similarly, the cross section for the dijet production is

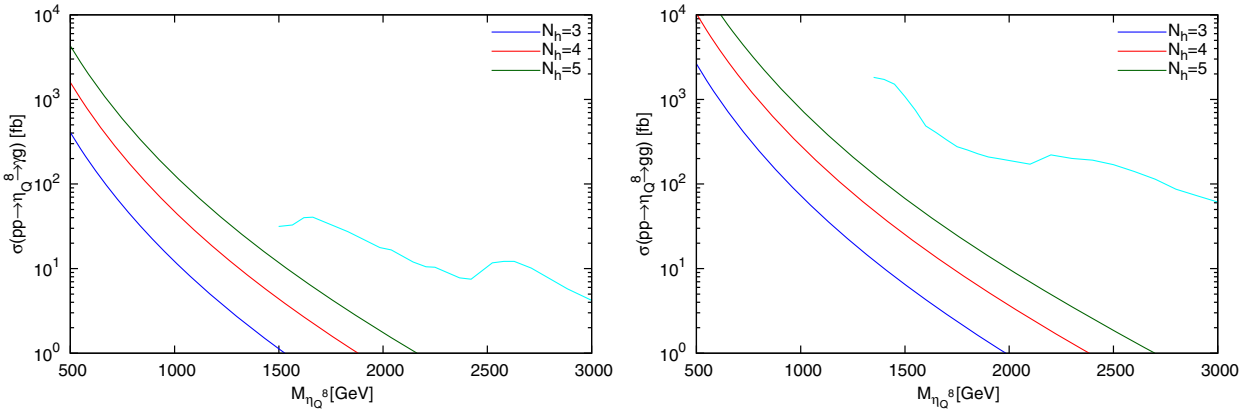

FIG. 5. The cross sections for (a) $pp \to \eta^8_{\tilde{Q}} \to \gamma g$ and (b) $pp \to \eta^8_{\tilde{Q}} \to gg$ in units of fb for $\alpha_h = 0.2$ as functions of $M_{\eta^8_{\tilde{Q}}}$ at the LHC with $\sqrt{s} = 13$ TeV. The cyan lines are the same experimental upper bounds used in Fig. 3.

$\sigma(pp \to \chi_{\tilde{Q}} \to q\bar{q}) \lesssim O(10^{-2})$ fb, which is not constrained by the data at all.

The scalar h-quarks can also make a QCD color-octet bound state but an h–color singlet. We denote such a ground state by $\eta^8_{\tilde{Q}}$, just like η^8_Q in the h-quark model. $\eta^8_{\tilde{Q}}$ can decay into gg, $g\gamma$, or Zg, where we suppress the three-body decay modes. The decay rates of the two-body modes are given by

$$\Gamma[\eta^8_{\tilde{Q}} \to gg] = \frac{(N_c^2-4)N_h\alpha_s^2}{16N_c m_{\tilde{Q}}^2}|R^8_{\eta_{\tilde{Q}}}(0)|^2, \tag{28}$$

$$\Gamma[\eta^8_{\tilde{Q}} \to \gamma g] = \frac{N_h\alpha_s\alpha e_{\tilde{Q}}^2}{2m_{\tilde{Q}}^2}|R^8_{\eta_{\tilde{Q}}}(0)|^2, \tag{29}$$

$$\Gamma[\eta^8_{\tilde{Q}} \to Zg] = \frac{N_h\alpha_s\alpha e_{\tilde{Q}}^2 x_w(4-r_Z)}{8(1-x_w)m_{\tilde{Q}}^2}|R^8_{\eta_{\tilde{Q}}}(0)|^2. \tag{30}$$

The branching ratios of the above decay channels are 0.70, 0.15, and 0.15, respectively. In Figs. 5(a) and 5(b), we show the production cross sections for $pp \to \eta^8_{\tilde{Q}} \to \gamma g$ and $pp \to \eta^8_{\tilde{Q}} \to gg$, respectively, in units of fb for $\alpha_h = 0.2$ as functions of $M_{\eta^8_{\tilde{Q}}}$ at $\sqrt{s} = 13$ TeV, compared with the same experimental bound (cyan lines) used in Fig. 3. We find that the expected cross sections in the scalar h-quark model are half of those in the h-quark model, and neither channel is constrained by the LHC data at $\sqrt{s} = 13$ TeV yet.

V. HOW TO DISTINGUISH A COMPOSITE $Q\bar{Q}$ FROM $\tilde{Q}\tilde{Q}^\dagger$

One of the key questions is how to distinguish η_Q from $\eta_{\tilde{Q}}$ if one finds a heavy diphoton resonance state in the near future at the LHC. This can be answered by noting that the J^{PC} quantum numbers of two states are different, namely 0^{-+} vs 0^{++}. Hence, the polarizations of two photons in the final states should be orthogonal vs parallel. A similar issue has been studied for the 125 GeV Higgs to determine its J^{PC} quantum numbers. For example, one can study the azimuthal angle distribution of the forward dijet in $gg \to \eta_Q(\text{or } \eta_{\tilde{Q}}) \to \gamma\gamma$. Furthermore, if the $gg \to \eta_Q(\text{or } \eta_{\tilde{Q}}) \to ZZ$ channel is kinematically allowed, one may study the J^{PC} quantum numbers of the scalar or pseudoscalar resonance via the angular distribution of decay products of the two Z bosons.

Another possible way to distinguish the two composite scenarios is via the DY production of the vector resonance ψ_Q or $\chi_{\tilde{Q}} \to l^+l^-$. As shown in Fig. 2, the predicted cross section for the DY production of $\psi_Q \to l^+l^-$ is 0.1–1 fb at $\sqrt{s} = 13$ TeV. On the other hand, we find that the cross section for the DY production of $\chi_{\tilde{Q}} \to l^+l^-$ is at most 10^{-4} fb at $\sqrt{s} = 13$ TeV. Therefore, the two ratios

$$\frac{\sigma(pp \to \psi_Q \to l^+l^-)}{\sigma(pp \to \eta_Q \to \gamma\gamma)} \text{vs} \frac{\sigma(pp \to \chi_{\tilde{Q}} \to l^+l^-)}{\sigma(pp \to \eta_{\tilde{Q}} \to \gamma\gamma)}, \tag{31}$$

in which some unknown factors such as N_h and the wave functions at the origin are canceled out, may prove to be useful in distinguishing between the two cases.

VI. INTERPRETATION OF DIPHOTON AND PHOTON + JET RESONANCES AS COMPOSITE SCALAR OR PSEUDOSCALAR AT THE LHC

Although there is no significant clue on any new physics at the LHC, there are a few resonant excesses with small significances deviated from SM predictions. In this section, we investigate the possibility that these small excesses might be interpreted as pseudoscalar or scalar composite particles, whose constituents are either new vectorlike quarks ($Q\bar{Q}$) or scalar quarks ($\tilde{Q}\tilde{Q}^\dagger$). In this section, we fix $N_h = 3$, but we set α_h and e_Q to be free.

A. Two diphoton resonances at 710 GeV and 1.6 TeV

At the 2016 ICHEP conference, both ATLAS [3] and CMS [4] reported new results on the 750 GeV diphoton excess, including new data in 2016. Combining the 2015 and 2016 data, the ATLAS Collaboration [3] observed a local significance of 2.3σ excess at 710 GeV with a large decay width to mass ratio, $\Gamma/M = 0.1$, and another one of 2.4σ at 1.6 TeV with a narrower width. On the other hand, the CMS Collaboration [4] has observed no significant excess by combining 2015 and 2016 data. In this section, we attempt to identify these small excesses in ATLAS data as signals of a pseudoscalar or scalar composite particle in the hypercolor model.

First, we consider the excess at 710 GeV. According to the MSTW2008NLO data [43], we have $C_{gg} = 2807$ and 237 at $\sqrt{s} = 13$ and 8 TeV, respectively. The expected value for the $\gamma\gamma$ signal at 710 GeV in the SM is about 1 fb, and it could reach about 2 fb with 2σ uncertainty [3]. In the following analysis, we interpret the 2.3σ local excess at 710 GeV as the production of η_Q or $\eta_{\tilde{Q}}$ decaying into $\gamma\gamma$, whose signal strength is taken to be less than 1.3 fb.

In Fig. 6, the cyan region corresponds to the region in which $\sigma(pp \to \eta_Q(\text{or } \eta_{\tilde{Q}}) \to \gamma\gamma) < 1.3$ fb when $\eta_{Q/\tilde{Q}} \to g_h g_h$ is allowed for the 710 GeV resonance. The gray region is ruled out by the bound from the search for a resonance decaying into a photon + jet at $\sqrt{s} = 8$ TeV in ATLAS data [73]. Explicitly, we set the bound $\sigma(pp \to \eta^8_{Q/\tilde{Q}} \to \gamma g) < 18$ fb for $M_{\eta_{Q/\tilde{Q}}} \sim 710$ GeV and $\Gamma/M \sim 5\%$ by assuming that the product of the efficiency and acceptance is 0.33 [9]. The dashed (dotted) line denotes the total decay width $\Gamma_{\eta_{Q/\tilde{Q}}}$/GeV corresponding to the ratio $\Gamma/M = 0.05$ (0.01).

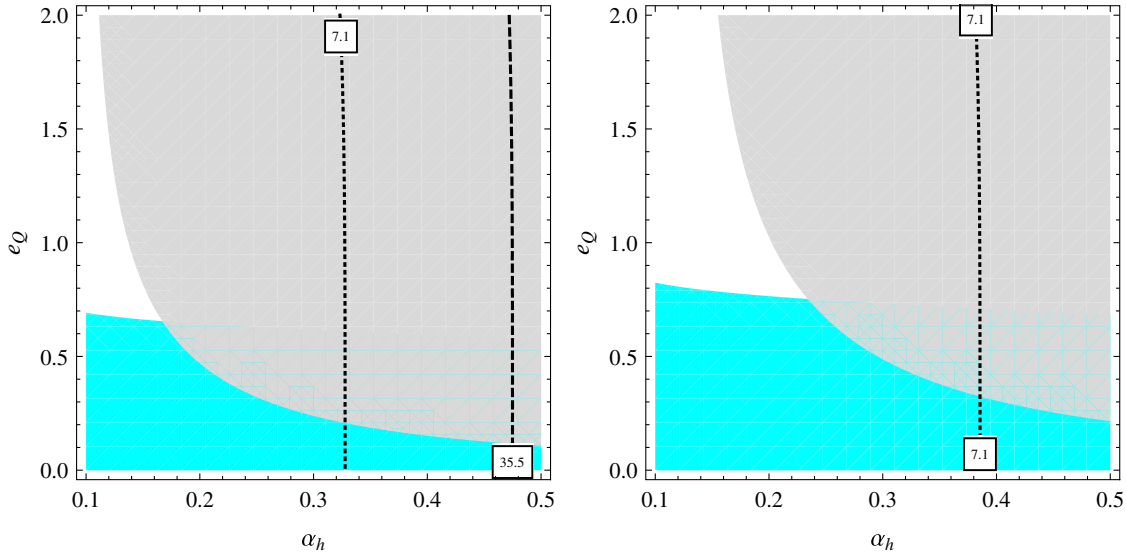

FIG. 6. The allowed region of α_h and e_Q for a resonance at 710 GeV in the diphoton channel at ATLAS [3]. The left (right) panel corresponds to the h-(scalar) quark model. The gray region is ruled out by the photon + jet search at $\sqrt{s} = 8$ TeV in ATLAS data [73]. The dashed (dotted) line denotes the total decay width $\Gamma_{\eta_{Q/\tilde{Q}}}$/GeV corresponding to the ratio $\Gamma/M = 0.05(0.01)$.

The left (right) panel in Fig. 6 corresponds to the case of η_Q ($\eta_{\tilde{Q}}$). In the h-scalar quark model, the allowed region is a little bit broader than in the h-quark model. Both models prefer the narrow decay width for the resonance so that the bound from the $\gamma +$ jet search might become stronger. There would be other constraints from the dijet, dilepton, ZZ, and $Z\gamma$ searches, but the constraints are much weaker than for the photon + jet search, as shown in Fig. 1.

Next, we consider the excess at 1.6 TeV. Here, $C_{gg} = 31.05$ and 1.18 at $\sqrt{s} = 13$ and 8 TeV, respectively. The expected value for the cross section times the branching ratio to $\gamma\gamma$ in the SM at 1.6 TeV is about 0.3 fb, and it could reach about 0.8 fb with 2σ uncertainty [3]. Therefore, we interpret the 2.4σ local excess at 1.6 TeV as the production of η_Q or $\eta_{\tilde{Q}}$ decaying into $\gamma\gamma$, whose cross section is less than 0.7 fb.

In Fig. 7, the cyan region corresponds to the region in which $\sigma(pp \to \eta_Q(\text{or } \eta_{\tilde{Q}}) \to \gamma\gamma) < 0.7$ fb when $\eta_{Q/\tilde{Q}} \to g_h g_h$ is kinematically allowed for the 1.6 TeV resonance. As in Fig. 6, the gray region is ruled out by the bound from the search for a resonance decaying into a photon + jet at $\sqrt{s} = 8$ TeV in ATLAS data [73], and we set the bound $\sigma(pp \to \eta^8_{Q/\tilde{Q}} \to \gamma g) < 4.2$ fb for $M_{\eta_{Q/\tilde{Q}}} = 1.6$ TeV and $\Gamma/M = 5\%$ by assuming that the product of the efficiency

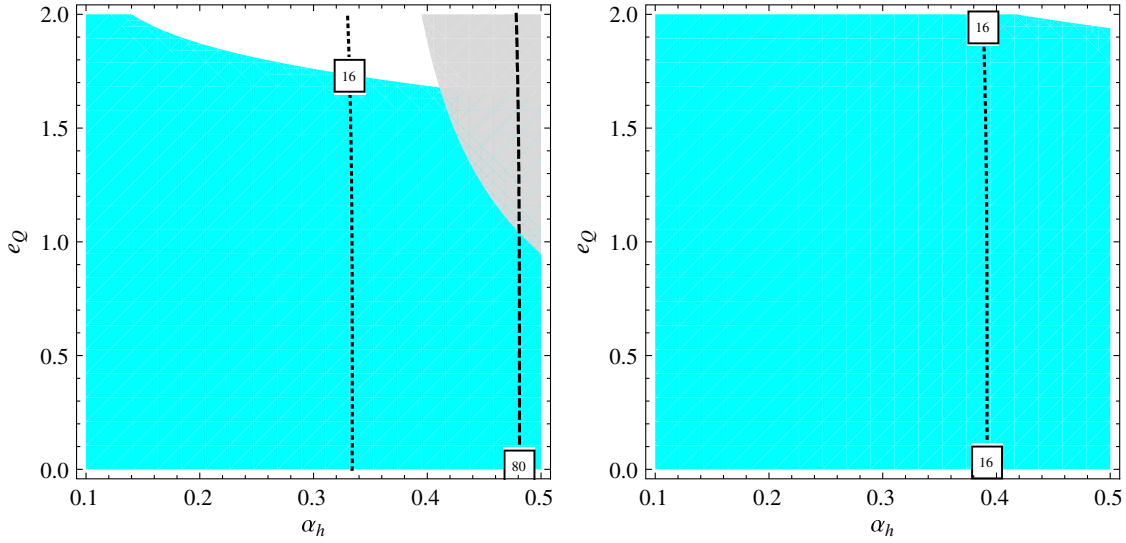

FIG. 7. Same as Fig. 6, for the 1.6 TeV resonance.

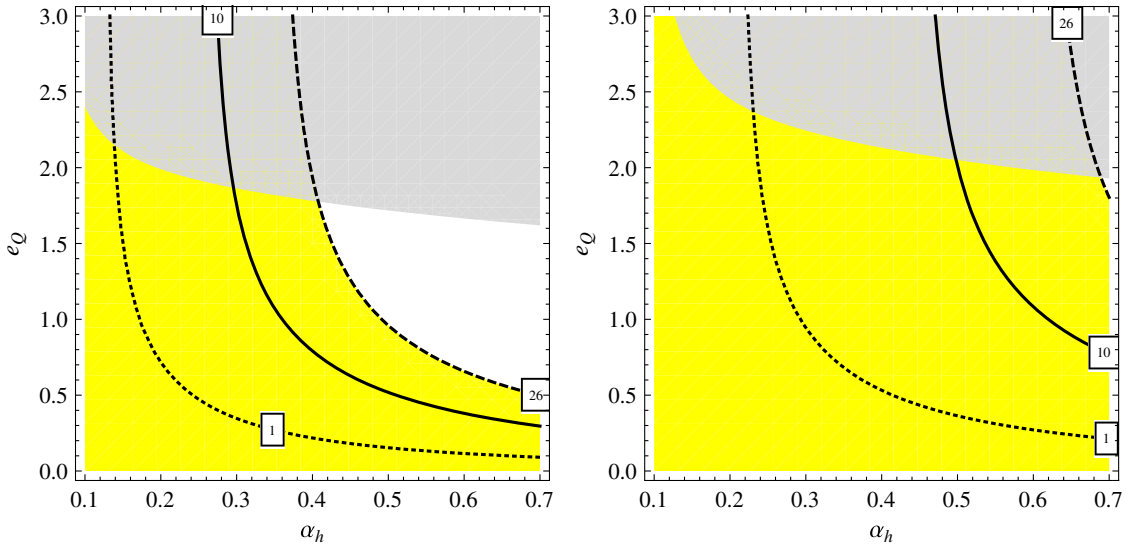

FIG. 8. The allowed region of α_h and e_Q for a resonance at 2 TeV in the photon + jet search at ATLAS [3]. The left (right) panel corresponds to the h-(scalar) quark model.

and acceptance is 0.33 [9]. Compared to the previous resonance at 710 GeV, the 1.6 TeV resonance has a much broader region of the parameter space and is less constrained by other LHC data.

B. γ + jet resonance at 2 TeV

The CMS Collaboration also announced that there might be some excess around 2 TeV in the photon + jet channel [74]. The largest deviation is seen at a mass of 2.0 TeV with a cross section about 45 fb, while the SM background expectation is about 19 fb [74]. Here, we interpret the excess as the production of the color-octet state, $\eta^8_{Q/\tilde{Q}}$ decaying into γg for $N_h = 3$, whose cross section is restricted to be less than 26 fb.

In the left (right) panel of Fig. 8, the yellow regions denote the allowed regions of α_h and e_Q for the η^8_Q ($\eta^8_{\tilde{Q}}$) case. The lines denote the contour values of the cross section for the photon+g production from the octet states. The gray regions are disfavored by the diphoton search at $\sqrt{s} = 13$ TeV by assuming that $\Gamma/M = 2\%$ in the ATLAS data [3], corresponding to the region where $\sigma(pp \to \gamma\gamma) > 0.2$ fb. In the scalar h-quark case (right), a much broader region is allowed, but it is impossible to achieve more than 10 fb for the cross section in the perturbative region. However, in the h-quark case (left), it is possible to achieve a cross section of 10 fb for $\alpha_h \sim 0.3$ and $e_Q \sim 1.5$.

VII. CONCLUSION

Diphoton or, in general, diboson resonance can play the role as a window to reveal new physics beyond the SM, like the existence of a hidden strongly interacting sector studied in this work.

In this paper, we have studied the possibility that a high-mass diphoton resonance is a composite scalar or pseudoscalar boson made up of $Q\bar{Q}$ or $\tilde{Q}\tilde{Q}^\dagger$. We have calculated the diphoton production cross section $pp \to \eta_Q(\eta_{\tilde{Q}}) \to \gamma\gamma$ and the Drell-Yan production cross section from $pp \to q\bar{q} \to \psi_Q(\chi_{\tilde{Q}}) \to l^+l^-$ at LHC 8 TeV. We found that the Drell-Yan production via ψ_Q at $\sqrt{s} = 8$ TeV has already been constrained for the scenario of $Q\bar{Q}$ bound state. We discussed how to distinguish the two composite scenarios by determining the J^{PC} of the scalar $\eta_{\tilde{Q}}$ or pseudoscalar η_Q diphoton resonance and using the Drell-Yan production of charged leptons of the ψ_Q or $\chi_{\tilde{Q}}$ resonance. The total decay width of η_Q or $\eta_{\tilde{Q}}$ can be either large or small depending on whether the $g_h g_h$ mode is open or closed. We note that the h-glueball case has been omitted in other similar analysis in the literature.

We interpreted the two small diphoton "excesses" at 710 GeV and 1.6 TeV reported by the LHC as the scalar or pseudoscalar composite in our model and determined the allowed regions of the parameter space from the data. We also found that existing photon + jet data from ATLAS impose strong constraints on the color-octet state η^8_Q or $\eta^8_{\tilde{Q}}$.

Besides the hyperquarkonia approach we are adopting here for the diboson resonances, there are many alternative composite interpretations as well. For example, in the composite Higgs model [31], the diboson resonances are considered as pNGBs. However, there are important distinctions between these two approaches using hyperquarkonia and pNGBs. The most notable distinction is that while the hyperquarkonia are formed by new strong confinement force, the pNGBs are coming from spontaneous symmetry breaking. Hence the mass differences between the lowest-lying state and excited states are

generally quasi-degenerated with mass differences less than 100 GeV or so in the former case, but large in the latter case. Moreover, in the hyperquarkonia approach, we can consider both fermionic and bosonic constituents in the new gauge group, while only fermionic constituents are possible to generate pNGBs. We have showed that one can use Drell-Yan to differentiate these two composite scenarios based on fermionic or bosonic constituents.

Finally, we note that for the case of h-quarks and scalar h-quarks forming $SU(2)_L$ doublets, general diboson resonances and even charged composites as discussed in Ref. [34] are also possible. P-wave scalar h-quark bound states are also interesting. These are all potentially relevant at LHC run II in the searches for new physics. We hope to report these results in more detail elsewhere [35].

ACKNOWLEDGMENTS

This work is supported in part by National Research Foundation of Korea (NRF) Research Grant No. NRF-2015R1A2A1A05001869, by the NRF grant funded by the Korea government (MSIP) (No. 2009-0083526) through the Korea Neutrino Research Center at Seoul National University (P. K.), and by the Ministry of Science and Technology (MoST) of Taiwan under Grant No. 101-2112-M-001-005-MY3 (C. Y. and T. C. Y.). The work of C. Y. is also supported in part by the Do-Yak project of NRF under Contract No. NRF-2015R1A2A1A15054533 and by the Basic Science Research Program through the National Research Foundation of Korea (NRF) funded by the Ministry of Science, ICT and Future Planning (No. 2017R1A2B4011946).

[1] M. Aaboud *et al.* (ATLAS Collaboration), Search for resonances in diphoton events at $\sqrt{s} = 13$ TeV with the ATLAS detector, J. High Energy Phys. 09 (2016) 001.
[2] V. Khachatryan *et al.* (CMS Collaboration), Search for Resonant Production of High-Mass Photon Pairs in Proton-Proton Collisions at $\sqrt{s} = 8$ and 13 TeV, Phys. Rev. Lett. **117**, 051802 (2016).
[3] ATLAS Collaboration, ATLAS Report No. ATLAS-CONF-2016-059, 2016.
[4] V. Khachatryan *et al.* (CMS Collaboration), Search for high-mass diphoton resonances in proton-proton collisions at 13 TeV and combination with 8 TeV search, Phys. Lett. B **767**, 147 (2017).
[5] M. x. Luo, K. Wang, T. Xu, L. Zhang, and G. Zhu, Squarkonium, diquarkonium, and octetonium at the LHC and their diphoton decays, Phys. Rev. D **93**, 055042 (2016).
[6] J. M. Cline and Z. Liu, LHC diphotons from electroweakly pair-produced composite pseudoscalars, arXiv:1512.06827.
[7] N. Craig, P. Draper, C. Kilic, and S. Thomas, Shedding light on diphoton resonances, Phys. Rev. D **93**, 115023 (2016).
[8] C. Han, K. Ichikawa, S. Matsumoto, M. M. Nojiri, and M. Takeuchi, Heavy fermion bound states for diphoton excess at 750 GeV: Collider and cosmological constraints, J. High Energy Phys. 04 (2016) 159.
[9] Y. Kats and M. J. Strassler, Resonances from QCD bound states and the 750 GeV diphoton excess, J. High Energy Phys. 05 (2016) 092; Erratum, J. High Energy Phys. 07 (2016) 44.
[10] J. F. Kamenik and M. Redi, Back to 1974: The $\mathcal{Q}$-onium, Phys. Lett. B **760**, 158 (2016).
[11] S. Iwamoto, G. Lee, Y. Shadmi, and R. Ziegler, Diphoton signals from colorless hidden quarkonia, Phys. Rev. D **94**, 015003 (2016).
[12] L. A. Anchordoqui, H. Goldberg, and X. Huang, Constraints on 750 GeV colorless Q-onia from running couplings, arXiv:1605.01937.
[13] R. Foot and J. Gargalionis, Explaining the 750 GeV diphoton excess with a colored scalar charged under a new confining gauge interaction, Phys. Rev. D **94**, 011703 (2016).
[14] K. Harigaya and Y. Nomura, Composite models for the 750 GeV diphoton excess, Phys. Lett. B **754**, 151 (2016).
[15] Y. Nakai, R. Sato, and K. Tobioka, Footprints of New Strong Dynamics via Anomaly and the 750 GeV Diphoton, Phys. Rev. Lett. **116**, 151802 (2016).
[16] S. Matsuzaki and K. Yamawaki, 750 GeV diphoton signal from one-family walking technipion, Mod. Phys. Lett. A **31**, 1630016 (2016).
[17] A. Belyaev, G. Cacciapaglia, H. Cai, T. Flacke, A. Parolini, and H. Serodio, Singlets in composite Higgs models in light of the LHC 750 GeV diphoton excess, Phys. Rev. D **94**, 015004 (2016).
[18] K. Harigaya and Y. Nomura, A composite model for the 750 GeV diphoton excess, J. High Energy Phys. 03 (2016) 091.
[19] K. Harigaya and Y. Nomura, Hidden pion varieties in composite models for diphoton resonances, Phys. Rev. D **94**, 075004 (2016).
[20] C. W. Chiang, M. Ibe, and T. T. Yanagida, Revisiting scalar quark hidden sector in light of 750-GeV diphoton resonance, J. High Energy Phys. 05 (2016) 084.
[21] N. D. Barrie, A. Kobakhidze, M. Talia, and L. Wu, 750 GeV composite axion as the LHC diphoton resonance, Phys. Lett. B **755**, 343 (2016).
[22] R. Nevzorov and A. W. Thomas, LHC signatures of neutral pseudo-Goldstone boson in the E6CHM, J. Phys. G **44**, 075003 (2017).
[23] J. M. Cline, W. Huang, and G. D. Moore, Challenges for models with composite states, Phys. Rev. D **94**, 055029 (2016).
[24] Y. Bai, V. Barger, and J. Berger, Constraints on color-octet companions of a 750 GeV heavy pion from dijet and photon

plus jet resonance searches, Phys. Rev. D **94**, 011701 (2016).
[25] A. Arbey, G. Cacciapaglia, H. Cai, A. Deandrea, S. Le Corre, and F. Sannino, Fundamental composite electroweak dynamics: Status at the LHC, Phys. Rev. D **95**, 015028 (2017).
[26] G. Cacciapaglia, H. Cai, A. Deandrea, T. Flacke, S. J. Lee, and A. Parolini, Composite scalars at the LHC: The Higgs, the sextet and the octet, J. High Energy Phys. 11 (2015) 201.
[27] G. Cacciapaglia, A. Deandrea, and M. Hashimoto, Scalar Hint from the Diboson Excess?, Phys. Rev. Lett. **115**, 171802 (2015).
[28] L. M. Carpenter and R. Colburn, Searching for Standard Model adjoint scalars with diboson resonance signatures, J. High Energy Phys. 12 (2015) 151.
[29] H. Cai, T. Flacke, and M. Lespinasse, A composite scalar hint from di-boson resonances?, arXiv:1512.04508.
[30] G. Ferretti, Gauge theories of partial compositeness: Scenarios for run-II of the LHC, J. High Energy Phys. 06 (2016) 107.
[31] A. Belyaev, G. Cacciapaglia, H. Cai, G. Ferretti, T. Flacke, A. Parolini, and H. Serodio, Di-boson signatures as standard candles for partial compositeness, J. High Energy Phys. 01 (2017) 094.
[32] C. Englert, P. Schichtel, and M. Spannowsky, Same-sign W pair production in composite Higgs models, Phys. Rev. D **95**, 055002 (2017).
[33] J. Kang and M. A. Luty, Macroscopic strings and "quirks" at colliders, J. High Energy Phys. 11 (2009) 065.
[34] K. Cheung, W. Y. Keung, and T. C. Yuan, Phenomenology of iquarkonium, Nucl. Phys. **B811**, 274 (2009).
[35] P. Ko, C. Yu, and T. C. Yuan (to be published).
[36] K. Hagiwara, K. Kato, A. D. Martin, and C. K. Ng, Properties of heavy quarkonia and related states, Nucl. Phys. **B344**, 1 (1990).
[37] P. Moxhay, Y. J. Ng, and S. H. H. Tye, The properties of scalar-quark bound states, Phys. Lett. B **158**, 170 (1985).
[38] Y. Chen *et al.*, Glueball spectrum and matrix elements on anisotropic lattices, Phys. Rev. D **73**, 014516 (2006).
[39] E. Gregory, A. Irving, B. Lucini, C. McNeile, A. Rago, C. Richards, and E. Rinaldi, Towards the glueball spectrum from unquenched lattice QCD, J. High Energy Phys. 10 (2012) 170.
[40] J. E. Juknevich, Pure-glue hidden valleys through the Higgs portal, J. High Energy Phys. 08 (2010) 121.
[41] G. T. Bodwin, E. Braaten, and G. P. Lepage, Rigorous QCD analysis of inclusive annihilation and production of heavy quarkonium, Phys. Rev. D **51**, 1125 (1995); Erratum, Phys. Rev. D **55**, 5853(E) (1997).
[42] R. Franceschini, G. F. Giudice, J. F. Kamenik, M. McCullough, A. Pomarol, R. Rattazzi, M. Redi, F. Riva, A. Strumia, and R. Torre, What is the $\gamma\gamma$ resonance at 750 GeV?, J. High Energy Phys. 03 (2016) 144.
[43] A. D. Martin, W. J. Stirling, R. S. Thorne, and G. Watt, Parton distributions for the LHC, Eur. Phys. J. C **63**, 189 (2009).
[44] ATLAS Collaboration, ATLAS Report No. ATLAS-CONF-2016-069, 2016.
[45] ATLAS Collaboration, ATLAS Report No. ATLAS-CONF-2016-055, 2016.
[46] ATLAS Collaboration, ATLAS Report No. ATLAS-CONF-2016-044, 2016.
[47] G. Aad *et al.* (ATLAS Collaboration), Search for high-mass diphoton resonances in pp collisions at $\sqrt{s} = 8$ TeV with the ATLAS detector, Phys. Rev. D **92**, 032004 (2015).
[48] CMS Collaboration, CMS Report No. CMS-PAS-EXO-12-045, 2015.
[49] CMS Collaboration, CMS Report No. CMS-PAS-EXO-16-018, 2016.
[50] G. Aad *et al.* (ATLAS Collaboration), Search for new phenomena in the dijet mass distribution using $p-p$ collision data at $\sqrt{s} = 8$ TeV with the ATLAS detector, Phys. Rev. D **91**, 052007 (2015).
[51] CMS Collaboration, CMS Report No. CMS-PAS-EXO-14-005, 2015.
[52] V. Khachatryan *et al.* (CMS Collaboration), Search for resonances and quantum black holes using dijet mass spectra in proton-proton collisions at $\sqrt{s} = 8$ TeV, Phys. Rev. D **91**, 052009 (2015).
[53] ATLAS Collaboration, ATLAS Report No. ATLAS-CONF-2016-030, 2016.
[54] CMS Collaboration, CMS Report No. CMS-PAS-EXO-16-032, 2016.
[55] G. Aad *et al.* (ATLAS Collaboration), Search for high-mass diboson resonances with boson-tagged jets in proton-proton collisions at $\sqrt{s} = 8$ TeV with the ATLAS detector, J. High Energy Phys. 12 (2015) 055.
[56] V. Khachatryan *et al.* (CMS Collaboration), Search for massive resonances decaying into pairs of boosted bosons in semi-leptonic final states at $\sqrt{s} = 8$ TeV, J. High Energy Phys. 08 (2014) 174.
[57] V. Khachatryan *et al.* (CMS Collaboration), Search for massive resonances in dijet systems containing jets tagged as W or Z boson decays in pp collisions at $\sqrt{s} = 8$ TeV, J. High Energy Phys. 08 (2014) 173.
[58] G. Aad *et al.* (ATLAS Collaboration), Search for an additional, heavy Higgs boson in the $H \to ZZ$ decay channel at $\sqrt{s} = 8$ TeV in pp collision data with the ATLAS detector, Eur. Phys. J. C **76**, 45 (2016).
[59] G. Aad *et al.* (ATLAS Collaboration), Search for resonant diboson production in the $\ell\ell q\bar{q}$ final state in pp collisions at $\sqrt{s} = 8$ TeV with the ATLAS detector, Eur. Phys. J. C **75**, 69 (2015).
[60] CMS Collaboration, CMS Report No. CMS-PAS-EXO-15-002, 2016.
[61] ATLAS Collaboration, ATLAS Report No. ATLAS-CONF-2016-079, 2016.
[62] ATLAS Collaboration, ATLAS Report No. ATLAS-CONF-2016-082, 2016.
[63] ATLAS Collaboration, ATLAS Report No. ATLAS-CONF-2016-056, 2016.
[64] CMS Collaboration, CMS Report No. CMS-PAS-B2G-16-010, 2016.
[65] CMS Collaboration, CMS Report No. CMS-PAS-HIG-16-033, 2016.
[66] G. Aad *et al.* (ATLAS Collaboration), Search for new resonances in $W\gamma$ and $Z\gamma$ final states in pp collisions at

$\sqrt{s} = 8$ TeV with the ATLAS detector, Phys. Lett. B **738**, 428 (2014).
[67] CMS Collaboration, CMS Report No. CMS-PAS-HIG-14-031, 2015.
[68] CMS Collaboration, CMS Report No. CMS-PAS-EXO-16-025, 2016.
[69] CMS Collaboration, CMS Report No. CMS-PAS-EXO-16-034, 2016.
[70] CMS Collaboration, CMS Report No. CMS-PAS-EXO-16-035, 2016.
[71] ATLAS Collaboration, ATLAS Report No. ATLAS-CONF-2016-045, 2016.
[72] G. Aad *et al.* (ATLAS Collaboration), Search for new phenomena with photon + jet events in proton-proton collisions at $\sqrt{s} = 13$ TeV with the ATLAS detector, J. High Energy Phys. 03 (2016) 041.
[73] G. Aad *et al.* (ATLAS Collaboration), Search for new phenomena in photon + jet events collected in proton-proton collisions at $\sqrt{s} = 8$ TeV with the ATLAS detector, Phys. Lett. B **728**, 562 (2014).
[74] CMS Collaboration, CMS Report No. CMS-PAS-EXO-16-015, 2016.
[75] G. Aad *et al.* (ATLAS Collaboration), Search for new phenomena in final states with an energetic jet and large missing transverse momentum in pp collisions at $\sqrt{s} = 8$ TeV with the ATLAS detector, Eur. Phys. J. C **75**, 299 (2015); Erratum, Eur. Phys. J. C **75**, 408(E) (2015).
[76] V. Khachatryan *et al.* (CMS Collaboration), Search for dark matter, extra dimensions, and unparticles in monojet events in proton-proton collisions at $\sqrt{s} = 8$ TeV, Eur. Phys. J. C **75**, 235 (2015).